

INTERPRETABLE ATTRIBUTED SCATTERING CENTER EXTRACTED VIA DEEP UNFOLDING

Haodong Yang¹, Zhe Zhang^{2,3}, Zhongling Huang^{1*}

¹School of Automation, Northwestern Polytechnical University

²Suzhou Aerospace Information Research Institute

³Aerospace Information Research Institute, Chinese Academy of Sciences (CAS)

ABSTRACT

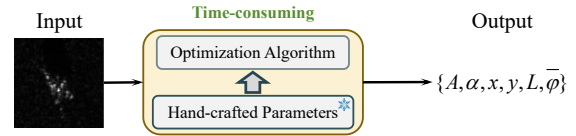
Most existing sparse representation-based approaches for attributed scattering center (ASC) extraction adopt traditional iterative optimization algorithms, which suffer from lengthy computation times and limited precision. This paper presents a solution by introducing an interpretable network that can effectively and rapidly extract ASC via deep unfolding. Initially, we create a dictionary containing reliable prior knowledge and apply it to the iterative shrinkage-thresholding algorithm (ISTA). Then, we unfold ISTA into a neural network, employing it to autonomously and precisely optimize the hyperparameters. The interpretability of physics is retained by applying a dictionary with physical meaning. The experiments are conducted on multiple test sets with diverse data distributions and demonstrate the superior performance and generalizability of our method.

Index Terms— Attributed Scattering Center, Deep Unfolding, Sparse Representation

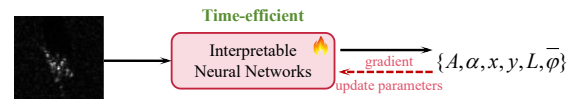
1. INTRODUCTION

Synthetic Aperture Radar (SAR) is an active microwave sensor capable of capturing images in all-day all-weather conditions. Since the capability of the ASC model to parameterize SAR target characteristics, there has been an increasing amount of research focused on extracting ASC [1, 2] and employing it for interpreting SAR data [3, 4].

The ASC parameter estimation process can be considered as a sparse representation problem due to the sparsity of radar echo. Several studies [1, 2] adopt sparse optimization methods to extract ASC, with the primary algorithms employed being orthogonal matching pursuit (OMP) [5], approximate message passing (AMP) [6] and ISTA [7]. As shown in Fig. 1 (a), traditional approaches frequently execute iterative optimization on single input data and require manual adjusting



(a) Traditional optimized algorithms for ASC extraction.



(b) Proposed interpretable neural networks.

Fig. 1. Compared with the traditional optimized algorithms and the proposed method for ASC extraction.

of hyperparameters. This will encounter issues such as inefficiency and imprecise results.

To tackle the aforementioned problems, we unfold ISTA into an interpretable neural network to achieve efficient and credible extraction of ASC, as shown in Fig. 1 (b). The main contributions are as follows:

1. We propose a novel approach via deep unfolding to extract ASC efficiently and precisely. In contrast to current deep unfolding methods employing random dictionaries [8], we utilize a dictionary that possesses physics prior information to enhance the model's interpretability.
2. Extensive experiments are conducted on the Moving and Stationary Target Acquisition and Recognition (MSTAR) dataset [9] to demonstrate the efficacy of the proposed method. Concretely, we train and validate the model using data at a depression angle of 17° , and then generalize it within data at depression angles of 15° and 45° . The results demonstrate the proposed approach has superior generalization.

*Corresponding Author.

This work was supported by the National Natural Science Foundation of China under Grant 62101459 and the China Postdoctoral Science Foundation under Grant BX2021248.

2. ATTRIBUTED SCATTERING CENTER MODEL

The ASC model is presented based on geometric theory diffraction and physical optics theory [10] to analyze the electromagnetic scattering response of the target. It can be viewed as a linear combination of N individual ASCs, each of which is regarded as a function of radar frequency f and aspect angle φ , where $f \in (f_c - B/2, f_c + B/2)$ and $\varphi \in (-\varphi_{syn}/2, \varphi_{syn}/2)$ with B , f_c and φ_{syn} denoting the bandwidth, the center frequency and the synthetic angle respectively. The ASC model at small angles can be modeled as follows [11]:

$$\begin{aligned} E(f, \varphi; \Theta) &= \sum_{i=1}^{K_0} E_i(f, \varphi; \theta_i) \\ &= \sum_{i=1}^{K_0} A_i \cdot \left(j \frac{f}{f_c}\right)^{\alpha_i} \\ &\quad \cdot \exp\left(-j \frac{4\pi f}{c} (x_i \cos \varphi + y_i \sin \varphi)\right) \end{aligned} \quad (1)$$

where E is the radar echo. $\Theta = [\theta_1, \theta_2, \dots, \theta_{K_0}]$ denotes the ASC parameter set and K_0 is the number of ASCs. E_i represents the i th ASC. $j = \sqrt{-1}$ indicates the imaginary unit and c is the propagation velocity. $\theta_i = \{A_i, \alpha_i, x_i, y_i\}$ is the i th ASC parameter set. A_i indicates the complex amplitude. x_i and y_i represent the coordinates in the range and azimuth directions, respectively. α reflects the frequency dependency factor that can distinguish the geometric structure.

Given the sparsity of radar echo in the ASC parameter space, the theory of sparse signal representation enables the analysis and extraction of ASC. Thus, the ASC model in Eq. 1 can be explained as below:

$$\tilde{s} = \tilde{\Phi}(\mathbf{x}, \mathbf{y})z \quad (2)$$

where \tilde{s} represents the vectorization of E and z is the sparse coefficient vector representing $A(j \frac{f}{f_c})^\alpha$ in Eq. 1. $\tilde{\Phi}$ indicates a parameterized dictionary that includes the position information of ASCs in the signal domain, which corresponds to the exponent term in Eq. 1. f and φ can be considered as vectors that are uniformly sampled P and Q times within their corresponding ranges, respectively. \mathbf{x} and \mathbf{y} are consistently sampled M and N times respectively. Thus, the dimensions of $\tilde{\Phi}$ are $PQ \times MN$. The dictionary can be formulated in columns as follows:

$$\begin{aligned} \tilde{\Phi}(\mathbf{x}, \mathbf{y}) &= \tilde{\Phi}_{:,1}, \tilde{\Phi}_{:,2}, \dots, \tilde{\Phi}_{:,MN}, \\ \tilde{\Phi}_{:,MN} &= \text{vec}\left(\exp\left(-j \frac{4\pi f}{c} (x_M \cos \varphi + y_N \sin \varphi)\right)\right). \end{aligned} \quad (3)$$

Considering the targets in MSTAR fall inside the central 80×80 , we construct the dictionary specifically for this region, in which the sampling numbers P , Q , M , and N are all set to 80. Fig. 2 illustrates the significance of each column in the dictionary within the image domain.

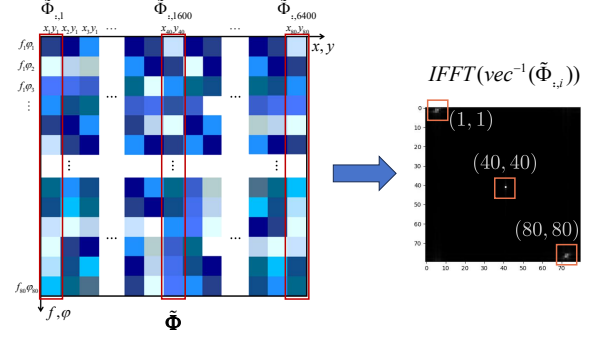


Fig. 2. The visualization of each column in the dictionary within the image domain.

Each column of the dictionary in the image domain can be represented as the scattering center of the corresponding coordinates via the Inverse Fast Fourier Transform (IFFT) and inverse vectorization, as illustrated in Fig. 2. Then the dictionary in the image domain can be approximated as a sparse matrix where the echo of each column is concentrated on the diagonal. Thus, extracting ASC in the image domain is essentially a matching problem.

Based on sparse representation theory, z can be solved in the image domain by the following step:

$$\arg \min_z \|\Phi z - s\|_2 + \lambda \|z\|_1, \quad (4)$$

where Φ and s are the dictionary in the image domain and the complex-valued image. λ is a hyperparameter. In this paper, we adopt ISTA to optimize it.

3. METHODS

In this section, we initially provide a concise overview of ISTA. Then we unfold it into a neural network and explain its operation. The architecture is shown in Fig. 3.

3.1. ISTA

ISTA is a widely utilized approach for proximal gradient descent that has been implemented in numerous problems involving sparse representation. It can be applied to solve the optimization problem presented in Eq. 4 by following the steps below:

$$\begin{aligned} x^{(k)} &= z^{(k-1)} - t \Phi^H (\Phi z^{(k-1)} - s), \\ z^{(k)} &= S_\rho(x^{(k)}). \end{aligned} \quad (5)$$

The variable k represents the index of the iteration, whereas t represents the step size. The soft-thresholding function for complex valued data, denoted as S_ρ , can be defined as follows:

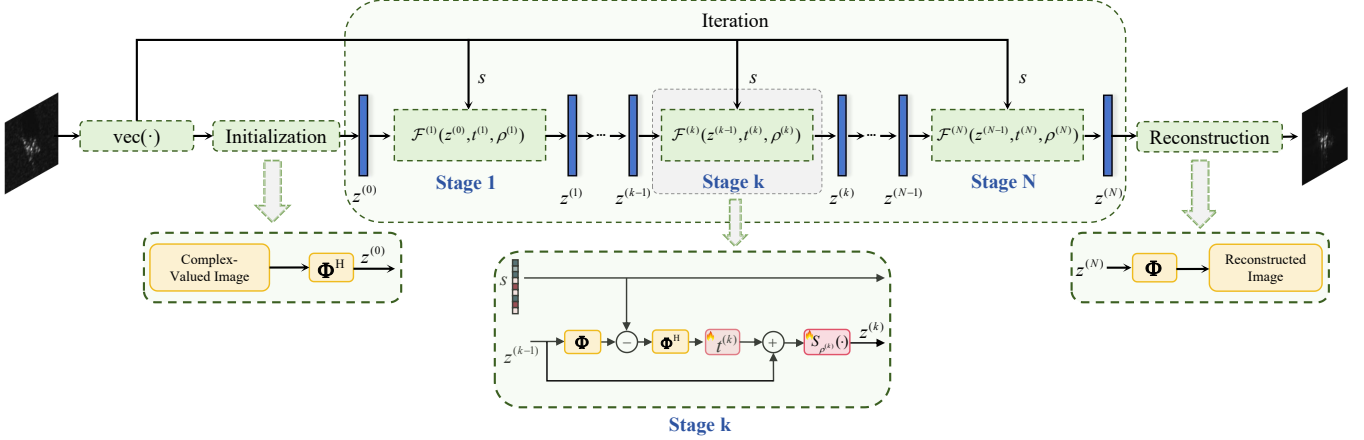


Fig. 3. The overall architecture of the proposed method.

$$S_{\rho}(x) = \text{sign}(x) \max(|x| - \rho, 0),$$

$$\text{sign}(x) = \begin{cases} \frac{x}{|x|}, & |x| > 0, \\ 0, & |x| = 0, \end{cases} \quad (6)$$

where ρ is a hyperparameter. The method requires hand-crafted parameters t and ρ based on the input s , resulting in a time-consuming and labor-intensive process.

3.2. Interpretable Unfolding ISTA

To perform efficient ASC parameter extraction, we unfold ISTA into a neural network and automatically optimize the hyperparameters. Different from existing deep unfolding methods [12, 13] that employ random matrices like Gaussian matrix as the dictionary, we adopt Φ as it encompasses physical information of radar echo. The proposed approach can be categorized into three phases: Initialization, Iteration, and Reconstruction, as depicted in Fig. 3.

Initialization. The complex-valued image is primarily vectorized before the initialization phase, denoted as s . The initial value $z^{(0)}$ of Stage 1 can be calculated as $z^{(0)} = \Phi^H s$.

Iteration. The iterative component consists of N analogous phases, with each phase being considered as an amplified version of ISTA. The internal intricacies of each phase are identical to those of Stage K depicted in the Fig. 3, which can be formulated as follows:

$$z^{(k)} = S_{\rho^{(k)}}(z^{(k-1)} + t^{(k)} \Phi^H (\Phi z^{(k-1)} - s)). \quad (7)$$

In contrast to traditional ISTA, we introduce t and ρ as trainable parameters in every stage. The quantity of parameters requiring updates and the inference time are contingent upon the overall stages N . We set N to be 4 empirically, resulting in 8 parameters total. The hyperparameters t and ρ for each stage are set to 0.01 and 0.005 respectively.

Reconstruction. The reconstructed image can be obtained by $z^{(N)}$ through the following procedures:

$$\hat{s} = \Phi z^{(N)}, \quad (8)$$

where \hat{s} denotes the reconstructed image. If $z^{(N)}$ is sufficiently sparse, then \hat{s} can be regarded as the outcome of eliminating the noisy regions of s while preserving the area with prominent scattering characteristics.

Following other deep unfolding methods [12, 13], we define the loss as follows for each sample:

$$\text{Loss} = \|s - \hat{s}\|_2 + \lambda \|z^{(N)}\|_1. \quad (9)$$

$\|s - \hat{s}\|_2$ indicates the residual loss, which is calculated by L2 normalization. $\lambda \|z^{(N)}\|_1$ serves as a regularization component. λ is a hyperparameter and is set to be 300 empirically.

4. EXPERIMENTS

4.1. Dataset and Experimental Settings

The experiments are conducted on the MSTAR dataset [9]. We randomly select 10% of the 17° depression angle samples as the training set and select another 10% of the remaining samples as the validation set. The test data for the 15° depression angle and the 45° depression angle are called D-15 and D-45 respectively.

We employ AdamW [14] along with the OneCycleLR [15] to optimize the model. The weight decay is 0.05 and the learning rate is $2e - 3$. The epoch and the batch size are 50 and 16 respectively. The studies are performed on a GeForce RTX 3090. The slices are normalized by the L2 normalization and center cropped to 80×80 .

4.2. Ablation Study

The residual loss and inference time on D-15 are documented in Table 1 as the number of network stages N increases incre-

Table 1. The residual loss and inference time with various N on D-15.

Stage Number	2	4	6	8
Residual Loss	0.6753	0.6617	0.6601	0.6603
Inference Time (s)	0.0616	0.0729	0.0887	0.0942

mentally. Once the number of stages surpasses 4, the decrease in residual loss becomes negligible, while the model inference time gradually grows. In summary, we decided to set N to 4 in the following experiments.

The images reconstructed within various λ are displayed in Fig. 4. As λ grows to 300, the background noise interference steadily reduces, resulting in an improvement in the quality of the reconstructed image. However, when λ is 500, it is over optimized. Therefore, λ is set to 300 in the following experiments.

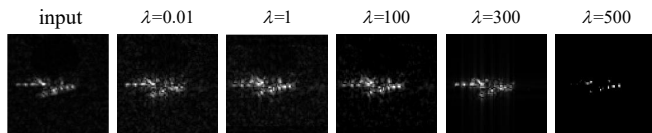


Fig. 4. The reconstruction image within various λ .

4.3. Comparison with Traditional Methods

Table 2 compares the proposed and traditional approaches on D-15, displaying average residual loss and inference time for each image. The sparsity of the OMP algorithm is 40. ISTA's t and ρ align with the unfolding network at 0.01 and 0.005, respectively. The change rate between adjacent iterations of the AMP is set to 0.1.

Table 2. The test results of various methods on D-15. The best are in **bold**.

Method	AMP	OMP	ISTA	Our method
Residual Loss	1.4993	1.1436	0.9440	0.6617
Inference Time (s)	84.5331	199.1839	73.6324	0.0729

Our method demonstrates a significant reduction in residual loss compared to traditional methods, ranging from 29.9% (compared to ISTA) to 55.9% (compared to OMP). In addition, our method can speed up the inference time by nearly 100 times ($73.6324 \rightarrow 0.0729$). Collectively, the proposed approach can extract ASC rapidly and precisely.

Fig. 5 presents the reconstructed images comparison between our method and traditional methods. It is evident that the proposed method outperforms the traditional algorithm in terms of accurately identifying and reconstructing the target area.

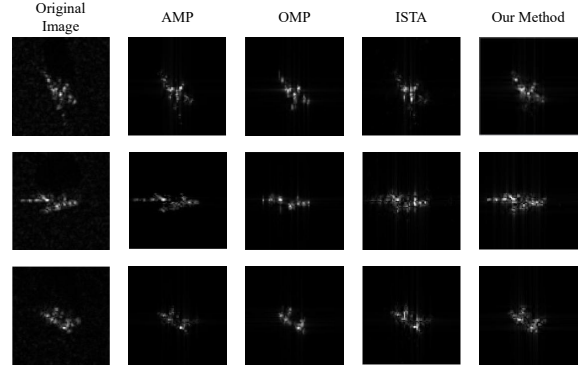


Fig. 5. Comparison of the reconstructed images between our method and traditional methods.

4.4. Model Generalization Discussion

Fig. 6 displays the ASC extraction results on D-45. It is worth noting that category A64 is not in the training set, as shown by the first three columns in the figure. The findings indicate that when the network is trained on data with a depression angle of 17° , it demonstrates impressive performance on the test set with a depression angle of 45° . Both the reconstruction image and the ASC visualization emphasize that the areas contain significant scattering characteristics, which demonstrates the exceptional ability of the model's generalization.

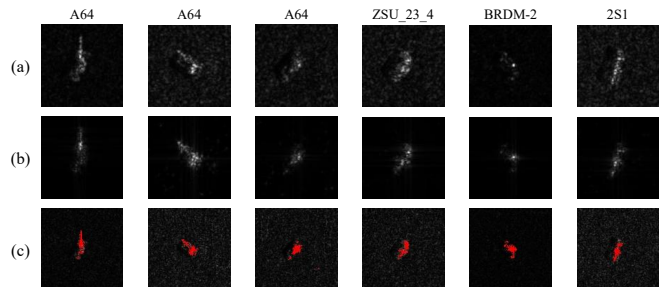


Fig. 6. The test results on D-45. (a)-(c) represents the original complex-valued image, the reconstructed image and the ASC visualization respectively.

5. CONCLUSION

Existing sparse representation theory-based ASC extraction methods adopt iterative optimization algorithms, which are slow and imprecise. We propose an interpretable deep unfolding method to achieve ASC extraction rapidly and precisely. Empirical evidence indicates that the proposed strategy can surpass traditional methods among test sets with diverse data distributions. Our future study will prioritize extracting the last parameters and acquiring all ASC parameter values.

6. REFERENCES

- [1] J. Wen and Z. Wang, "A new method for parameter estimation of attributed scattering centers based on amplitude-phase separation," *Journal of Radars*, vol. 8, no. 5, pp. 606–615, 2019.
- [2] F. Li, B. Jiu, H. Liu, Y. Wang, and L. Zhang, "Sparse representation based algorithm for estimation of attributed scattering center parameter on sar imagery," *Journal of Electronics & Information Technology*, vol. 36, no. 4, pp. 931–937, 2014.
- [3] Z. Huang, C. Wu, X. Yao, Z. Zhao, X. Huang, and J. Han, "Physics inspired hybrid attention for sar target recognition," *ISPRS Journal of Photogrammetry and Remote Sensing*, vol. 207, pp. 164–174, 2024.
- [4] Z. Huang, C. Wu, X. Yao, L. Wang, and J. Han, "Physically explainable intelligent perception and application of sar target characteristics based on time-frequency analysis," *Journal of Radars*, vol. 12, pp. 1–14, 2023.
- [5] J. A. Tropp and A. C. Gilbert, "Signal recovery from random measurements via orthogonal matching pursuit," *IEEE Transactions on information theory*, vol. 53, no. 12, pp. 4655–4666, 2007.
- [6] D. L. Donoho, A. Maleki, and A. Montanari, "Message-passing algorithms for compressed sensing," *Proceedings of the National Academy of Sciences*, vol. 106, no. 45, pp. 18914–18919, 2009.
- [7] T. Blumensath and M. E. Davies, "Iterative thresholding for sparse approximations," *Journal of Fourier analysis and Applications*, vol. 14, pp. 629–654, 2008.
- [8] J. Zhang, B. Chen, R. Xiong, and Y. Zhang, "Physics-inspired compressive sensing: Beyond deep unrolling," *IEEE Signal Processing Magazine*, vol. 40, no. 1, pp. 58–72, 2023.
- [9] Sandia National Laboratory, "The Air Force Moving and Stationary Target Recognition Database," <https://www.sdms.afrl.af.mil/index.php?collection=mstar>, Accessed May 2023.
- [10] M. J. Gerry, L. C. Potter, I. J. Gupta, and A. Van Der Merwe, "A parametric model for synthetic aperture radar measurements," *IEEE transactions on antennas and propagation*, vol. 47, no. 7, pp. 1179–1188, 1999.
- [11] M. Xing, Y. Xie, Y. Gao, J. Zhang, J. Liu, and Z. Wu, "Electromagnetic scattering characteristic extraction and imaging recognition algorithm: A review," *Journal of Radars*, vol. 11, no. 6, pp. 921–942, 2022.
- [12] J. Zhang and B. Ghanem, "Ista-net: Interpretable optimization-inspired deep network for image compressive sensing," in *Proceedings of the IEEE conference on computer vision and pattern recognition*, 2018, pp. 1828–1837.
- [13] Z. Zhang, Y. Liu, J. Liu, F. Wen, and C. Zhu, "Amp-net: Denoising-based deep unfolding for compressive image sensing," *IEEE Transactions on Image Processing*, vol. 30, pp. 1487–1500, 2020.
- [14] I. Loshchilov and F. Hutter, "Decoupled weight decay regularization," *arXiv preprint arXiv:1711.05101*, 2019.
- [15] L. N. Smith and N. Topin, "Super-convergence: Very fast training of neural networks using large learning rates," vol. 11006, pp. 369–386, 2019.